ELSEVIER

Coastal Engineering 36 (1999) 17–36

COASTAL ENGINEERING

A locally nonlinear interpretation of PUV measurements

Rodney J. Sobey [a,*], Steven A. Hughes [b]

[a] *Department of Civil and Environmental Engineering, University of California, 539 Davis Hall, Berkeley, CA 94720-1710, USA*

[b] *Coastal and Hydraulics Laboratory, USAE Waterways Experiment Station, Vicksburg, MS 39180, USA*

Received 5 May 1998; revised 19 October 1998; accepted 27 October 1998

Abstract

A time domain method is presented for analyzing simultaneous measurements of pressure and the horizontal components of velocity obtained beneath irregular multidirectional wave fields. This new method differs from the usual linear directional analyses applied to PUV data in two important aspects. First, the essential nonlinearity of the measured waves is not sacrificed to achieve a solution. Therefore, predictions of sea surface elevation and directional kinematics throughout the water column accurately portray the actual nonlinear character of the waves. Second, the analysis method is 'local' in that it can be applied to segments of PUV time series much shorter than an individual wave. The viability of the locally nonlinear methodology developed in this paper is proven by demonstrating agreement with higher-order theoretical steady waves. Predictions of sea surface elevation and wave kinematics are also made using actual measurements from PUV instruments at two ocean sites off the west coast of the United States.
© 1999 Elsevier Science B.V. All rights reserved.

Keywords: Data processing; Marine environment; Mathematical methods; Measurements; Ocean waves; Time domain analysis

1. Introduction

The PUV gauge has been a popular field instrument for sensing the directional characteristics of waves. It groups together a pressure transducer and a directional

* Corresponding author. Tel.: +1-510-6423162; Fax: +1-510-6438934; E-mail: sobey@ce.berkeley.edu

0378-3839/99/$ - see front matter © 1999 Elsevier Science B.V. All rights reserved.
PII: S0378-3839(98)00047-7

current meter in an assemblage such that both instruments have the same horizontal position and adjacent but wholly submerged vertical positions. In shallow waters, this assemblage would commonly be deployed near the bed. In deeper waters, deployment may be much higher in the water column, because of the considerable attenuation in signal magnitudes with depth. Because these gauges are not surface-piercing, they escape the most extreme environmental conditions and have the potential to optimize data recovery.

The PUV gauges provide simultaneous traces of submerged pressure $p(t;x_\alpha,z_\mathrm{P})$ and submerged horizontal velocity components (u,v) or $u_\alpha(t;x_\alpha,z_\mathrm{UV})$. Both instruments are at the same fixed horizontal position (x,y) or x_α but at different (though fixed and adjacent) vertical elevations z_P and z_UV, respectively, as sketched in Fig. 1. For notation convenience, the horizontal tensor notation will be adopted; the position coordinates are (x_α,z) and the velocity coordinates (u_α,w), with $\alpha=1$ and $\alpha=2$ corresponding to the x and y directions, respectively, of a cartesian coordinate system. The z-axis is directed vertically upwards from the horizontal plane of the local mean water level (MWL), in opposition to the gravity vector $\vec{g}$.

Short extracts from two measured PUV traces are shown in Fig. 2. Trace (a) was measured in 46 m of water at Platform Edith, about 9 km offshore from Huntington Beach, southern California. To a MWL datum, both the pressure gauge and the directional current meter are at -7.4 m. The sampling rate is 1 Hz. Trace (b) was measured in 17.6 m of water off the Columbia River on the Pacific coast of the United States. To a MWL datum, both the pressure gauge and the directional current meter are at -16.8 m. The sampling rate is 4 Hz. There is a substantial ambient current in record (b).

Although combined into a single instrument, the precision and response of the pressure and directional current sensors are not identical. It is immediately clear from Fig. 2 that there is significant instrument noise in the UV traces; this is especially

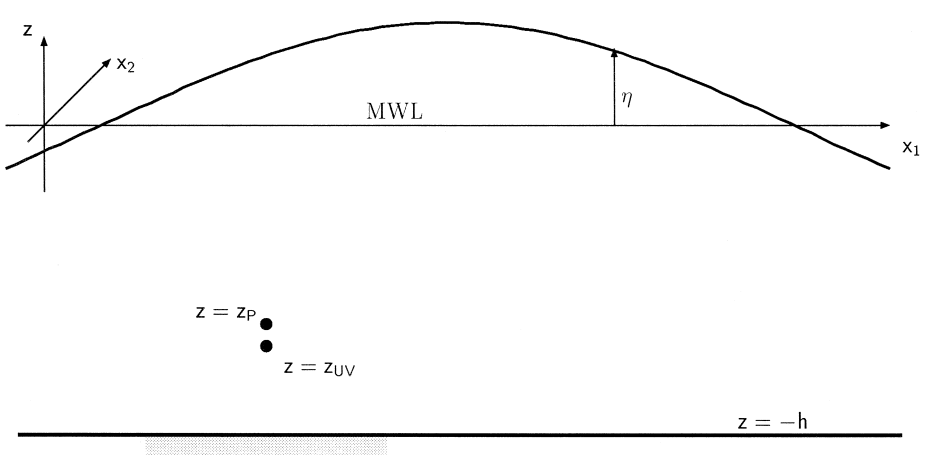

Fig. 1. Definition sketch and PUV gauge location.

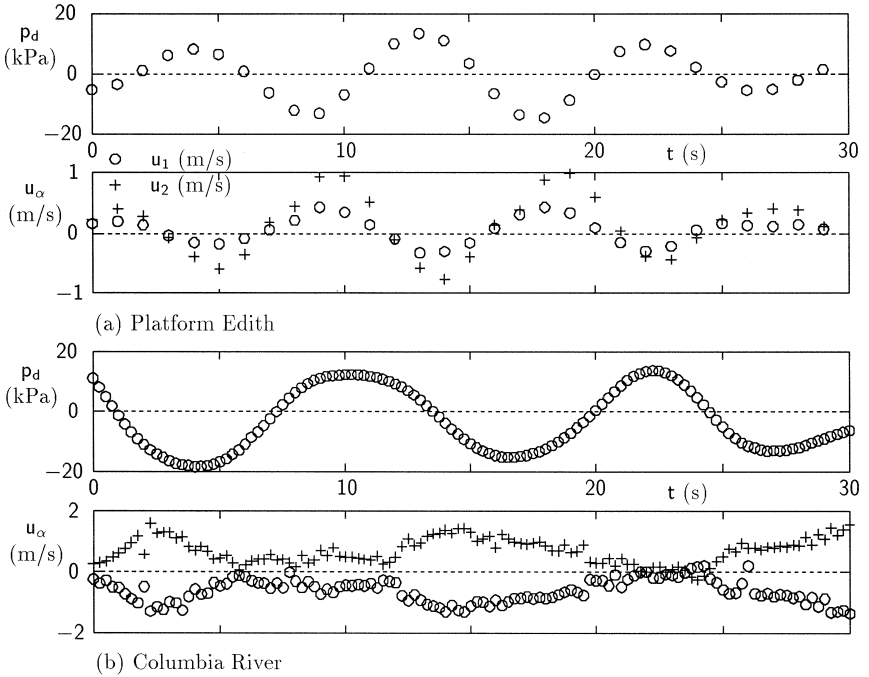

Fig. 2. Measured PUV traces.

notable in trace (b) where the sampling interval is much shorter. The P traces are consistently smooth. In addition, time is measured independently by each sensor, and systematic timing discrepancies are possible. This is not evident at the scale of these plots, but becomes a potential concern at the time scale of the local analysis that is subsequently outlined.

Analysis of simultaneous traces such as Fig. 2 has routinely adopted linear wave theory in the interpretation of the local kinematics and in the estimation of the water surface time history. This prior assumption of linearity has the potential for significant misinterpretation of the actual local kinematics. Nonlinear influences may be filtered and distorted by the record interpretation. In addition, most linear analyses assume stationary conditions over a measurement span of sufficient duration to obtain adequate frequency resolution in the Fourier transform.

This paper will introduce and demonstrate a nonlinear theory for the interpretation of PUV traces. The initial discussion will review and illustrate the common linear analysis. This leads to the presentation of a nonlinear theory for the interpretation of the local irregular kinematics sampled by the PUV gauge. The theory follows the spirit of the Sobey (1992) analysis for irregular wave kinematics from a water surface record. The nonlinear PUV theory is demonstrated and evaluated for theoretical PUV traces from steady wave theory and for measured PUV traces from the Platform Edith and Columbia River sites anticipated in Fig. 2.

2. Global linear analysis

Linear analyses of direction-sensing field instruments have mostly followed the floating buoy analysis of Longuet-Higgins et al. (1963) (see also Horikawa, 1988). This is a frequency domain analysis, which uses the entire burst sample for each kinematic quantity measured. A typical burst sample has a duration of about 20 min, such that it would include upwards of a hundred waves. There are essentially equivalent implementations in the time domain (e.g., Lee and Wang, 1984).

The fundamental basis of the methodology is the Gaussian random wave model, in which the irregular water surface is represented as the superposition of very many linear waves of different frequencies, directions and amplitudes. In the limit, summing over all positive frequencies ω and directions θ, the water surface η is represented as:

$$\eta(x_\alpha,t) = \frac{1}{2\pi}\int_{-\pi}^{\pi}\int_0^\infty F(\omega,\theta)\exp\left[-i(k_\alpha x_\alpha - \omega t)\right]\mathrm{d}\omega\mathrm{d}\theta, \tag{1}$$

where $F(\omega,\theta)$ is the complex Fourier transform of η in radian frequency-direction space, defined by the inverse Fourier transform:

$$F(\omega,\theta;x_\alpha,t) = \int_{-\pi}^{\pi}\int_0^\infty \eta(x_\alpha,t)\exp\left[i(k_\alpha x_\alpha - \omega t)\right]\mathrm{d}\omega\mathrm{d}\theta, \tag{2}$$

and k_α are the cartesian components of the vector wave number $\vec{k}$. k_α and ω are related through the linear dispersion relationship for waves on a steady current:

$$(\omega - k_\alpha U_\alpha)^2 = gk\tanh kh, \tag{3}$$

in which U_α is the local depth-uniform and steady current.

It follows directly from linear wave theory that the Fourier transforms of the dynamic pressure p_d and the horizontal velocity components u_α are:

$$F_p(\omega,\theta;x_\alpha,z,t) = K_p(\omega;z)F(\omega,\theta;x_\alpha,t), \tag{4}$$

$$F_{u_\alpha}(\omega,\theta;x_\alpha,z,t) = K_u(\omega;z)\frac{k_\alpha}{k}F(\omega,\theta;x_\alpha,t), \tag{5}$$

respectively, where k_α/k is the vector (cos θ, sin θ) and:

$$K_p(\omega;z) = \rho g\frac{\cosh k(h+z)}{\cosh kh} \text{ and } K_u(\omega;z) = (\omega - k_\alpha U_\alpha)\frac{\cosh k(h+z)}{\sinh kh}. \tag{6}$$

The K_p and K_u transfer functions are not dependent on the observations. In practice, the Doppler adjustment for local current is mostly omitted, a common practice being to remove the mean level (i.e., the current) from the velocity traces prior to analysis.

Longuet-Higgins et al. (1963) approximated the local directional variance spectrum $E(\omega,\theta)$, strictly $E_{\eta\eta}(\omega,\theta)$, as the first five terms in a Fourier series in θ:

$$E(\omega,\theta) = a_0 + \frac{2}{3}(a_1\cos\theta + b_1\sin\theta) + \frac{1}{6}(a_2\cos 2\theta + b_2\sin 2\theta) + \ldots \tag{7}$$

in which (Grosskopf et al., 1983; Horikawa, 1988) the coefficients are frequency-dependent:

$$a_0(\omega) = \frac{E_{pp}(\omega)}{2\pi K_p^2(\omega; z_P)} \tag{8}$$

$$a_1(\omega) = \frac{E_{pu_1}(\omega)}{\pi K_p(\omega; z_P) K_u(\omega; z_{UV})} \qquad a_2(\omega) = \frac{E_{u_1u_1}(\omega) - E_{u_2u_2}(\omega)}{\pi K_u^2(\omega; z_{UV})} \tag{9}$$

$$b_1(\omega) = \frac{E_{pu_2}(\omega)}{\pi K_p(\omega; z_P) K_u(\omega; z_{UV})} \qquad b_2(\omega) = \frac{2E_{u_1u_2}(\omega)}{\pi K_u^2(\omega; z_{UV})}. \tag{10}$$

$E_{pp}(\omega)$, $E_{u_1u_1}(\omega)$ and $E_{u_2u_2}(\omega)$ are the auto-variance spectra estimated from the p, u_1 and u_2 burst samples. $E_{pu_1}(\omega)$, $E_{pu_2}(\omega)$ and $E_{u_1u_2}(\omega)$ are the cross-variance spectra from the same burst samples.

This algorithm has the advantages of convenience, relative simplicity and many years of routine use. The fundamental reliance on linear theory and on spectral analysis are both potentially significant constraints. Linear theory compromises the identification and extraction of nonlinear influences in the data. The practice of spectral analysis insists that the local kinematics at time t be dependent with almost equal weight on all data observations at $t = 0, \Delta t, 2\Delta t, 3\Delta t, \ldots, (N-1)\Delta t$ in the burst sample. For PUV data, Δt is typically 1 s and the $N\Delta t$ duration of the data is typically 20 min, for which N exceeds 1000 observations. This is a linear and very global (burst-sample duration) interpretation. To preserve the physical integrity of the data, a very local interpretation would be preferable. Locally linear and then locally nonlinear theories are presented in the following sections.

3. A local linear analysis

A linear but locally focused interpretation is a useful intermediate step, in the spirit of the Nielsen (1989) locally linear approximation to irregular wave kinematics from a water surface trace. The basis is linear theory estimates of dynamic pressure and horizontal velocity components:

$$p_d(x_\alpha, z, t) = \rho g \frac{\cosh k(h+z)}{\cosh kh} \eta(x_\alpha, t), \tag{11}$$

$$u_\alpha(x_\alpha, z, t) = U_\alpha + \frac{k_\alpha}{k}(\omega - k_\alpha U_\alpha) \frac{\cosh k(h+z)}{\sinh kh} \eta(x_\alpha, t), \tag{12}$$

in which:

$$\eta(x_\alpha, t) = a\cos(k_\alpha x_\alpha - \omega t), \tag{13}$$

is the linear water surface, and k and ω are related through the linear dispersion relationship (Eq. (3)).

A prediction of the local kinematics is sought throughout the water column in the immediate neighborhood of the PUV gauge at horizontal position x_α. The pressure sensor is at known elevation z_P and the directional current meter at known elevation z_{UV}. Measured dynamic pressure traces $p_d^{obs} = p_d(t_i; x_\alpha, z_P)$ are available at discrete times t_i, as are measured velocity component traces $u_\alpha^{obs} = u_\alpha(t_i; x_\alpha, z_{UV})$ at the same discrete times. The local water depth h and depth-uniform current U_α are also known. The current can be estimated from the UV traces as a time-average over sufficient time to average over the local waves but not over local astronomical and storm tide currents.

At each time, there are four unknowns (ω, k_α and η) and four equations, dispersion (Eq. (3)) plus the three observational equations (Eqs. (11) and (12)). These are the simultaneous implicit algebraic equations:

$$\begin{aligned}
f_1(\omega, k_\alpha, \eta) &= (\omega - k_\alpha U_\alpha)^2 - gk \tanh kh = 0 \\
f_2(\omega, k_\alpha, \eta) &= \rho g \frac{\cosh k(h + z_P)}{\cosh kh} \eta - p_d^{obs} = 0 \\
f_3(\omega, k_\alpha, \eta) &= U_1 + \frac{k_1}{k}(\omega - k_\alpha U_\alpha) \frac{\cosh k(h + z_{UV})}{\sinh kh} \eta - u_1^{obs} = 0 \\
f_4(\omega, k_\alpha, \eta) &= U_2 + \frac{k_2}{k}(\omega - k_\alpha U_\alpha) \frac{\cosh k(h + z_{UV})}{\sinh kh} \eta - u_2^{obs} = 0,
\end{aligned} \tag{14}$$

In principle, a unique local solution at each time t_i can be computed. An analytical solution does not seem feasible. A direct numerical algorithm is the Newton–Raphson method. Writing Eq. (14) as $f_i(x_j) = 0$ where $i, j = 1,2,3,4$ and vector $\boldsymbol{x}_j^{(n)}$ as the solution estimate at iteration n, the correction $\Delta \boldsymbol{x}_j^{(n)}$ is suggested by the local Taylor series expansion:

$$f_i\left(\boldsymbol{x}_j^{(n)}\right) + \left.\frac{\partial f_i}{\partial x_j}\right|^{(n)} \Delta \boldsymbol{x}_j^{(n)} + \ldots = 0. \tag{15}$$

The Jacobian $\partial f_i / \partial x_j$ is evaluated analytically and Eq. (15) is solved by matrix inversion.

The predictive potential of this algorithm was evaluated for a theoretical steady wave train of period 10 s and height 10 m, directed at $+\pi/10$ to the x-axis in 20 m of water and an opposing current of -1 m/s. The PUV gauge is located at $z_P = z_{UV} = -10$ m. The initial theoretical PUV trace was computed from Airy theory at a sampling time interval of 0.5 s. With this trace as the measured PUV record, the local linear algorithm predicted the local wave frequency, the local wave number components and the local water surface elevation. Except in the immediate neighborhood of zero-crossings, where profile curvature is minimal and Eq. (14) is ill-conditioned, there was consistent agreement with Airy theory to four significant figures.

A second theoretical PUV trace (record 'Twenty'; see Table 1) was computed from near-exact (global) Fourier wave theory (Sobey, 1989), also at a sampling time interval of 0.5 s. With this trace as the measured PUV record, the local linear algorithm was significantly less successful.

Table 1
Sample theoretical waves

Wave	H	h	T	U_1	U_2	z_P	z_{UV}
Five	3 m	5 m	10 s	−1.902	−0.618	−5.0 m	−5.0 m
Twenty	10 m	20 m	10 s	−0.951	−0.309	−10.0 m	−10.0 m
Hundred	20 m	100 m	10 s	−0.478	−0.155	−20.0 m	−20.0 m

The predicted water surface elevation and wave number components from the local linear algorithm are shown in Fig. 3 as the markers, together with the near-exact predictions from global Fourier wave theory as the solid lines. Solutions to Eq. (14) at times in the immediate neighborhood of the zero-crossings were difficult to obtain, and required initial solution estimates that were almost exact. For this 'wave transitional' situation, a solution was obtained throughout. It is smooth and visually convincing, except when compared with the near-exact predictions. There is order of magnitude agreement only. The crest elevation in particular is poorly predicted.

Some variations on the locally linear formulation may achieve a more acceptable and perhaps also more robust local solution, but the indications are not encouraging. Eliminating η between the f_2 and both the f_3 and f_4 equations gives:

$$\frac{k_\alpha}{k}(\omega - k_\alpha U_\alpha) = \left(u_\alpha^{\text{obs}} - U_\alpha\right)\frac{\rho g}{p_{\text{d}}^{\text{obs}}}\frac{\cosh k(h + z_{\text{P}})}{\cosh k(h + z_{\text{UV}})}\tanh kh. \tag{16}$$

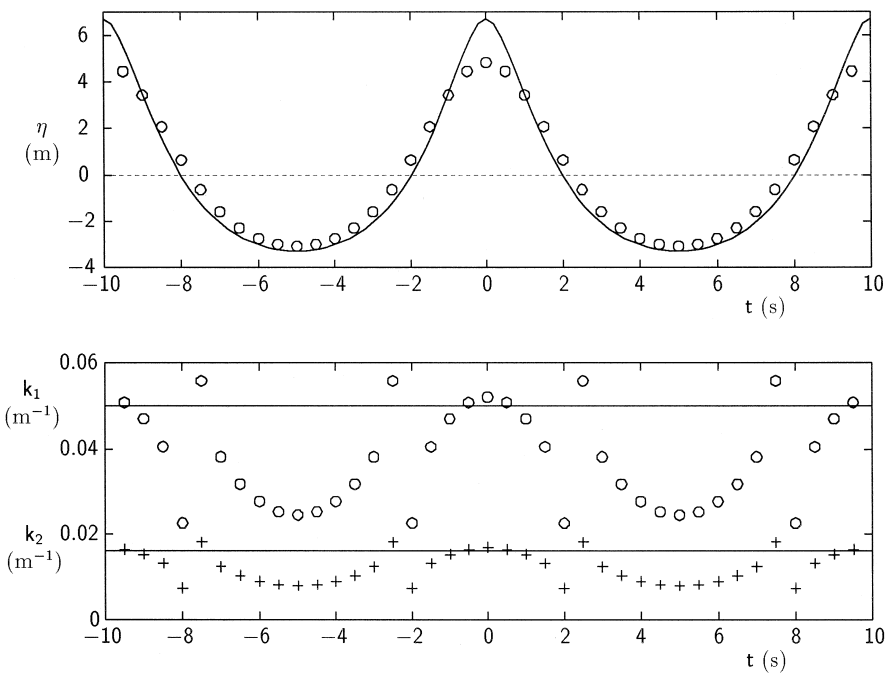

Fig. 3. Local linear theory (markers) and global Fourier theory (solid lines) predictions for Record 'Twenty'.

Squaring now and using in the f_1 equation establishes a single implicit algebraic equation in the local wave number k:

$$F(k) = \left(u_\alpha^{\text{obs}} - U_\alpha\right)\left(u_\alpha^{\text{obs}} - U_\alpha\right)\left[\frac{\rho g}{p_{\text{d}}^{\text{obs}}}\frac{\cosh k(h + z_{\text{P}})}{\cosh k(h + z_{\text{UV}})}\right]^2 - \frac{gk}{\tanh kh} = 0. \quad (17)$$

Some special cases of this equation are very revealing. When $z_{\text{P}} = z_{\text{UV}}$, Eq. (17) becomes:

$$F'(k) = \frac{1}{gh}\left(u_\alpha^{\text{obs}} - U_\alpha\right)\left(u_\alpha^{\text{obs}} - U_\alpha\right)\left[\frac{\rho g}{p_{\text{d}}^{\text{obs}}}\right]^2 - \frac{kh}{\tanh kh} = 0. \quad (18)$$

The function $kh/\tanh\ kh$ is 1 at $kh = 0$ ('wave shallow' water), and approaches kh asymptotically from above for large kh ('wave deep' water). There are solutions only for:

$$\frac{1}{gh}\left(u_\alpha^{\text{obs}} - U_\alpha\right)\left(u_\alpha^{\text{obs}} - U_\alpha\right)\left[\frac{\rho g}{p_{\text{d}}^{\text{obs}}}\right]^2 > 1. \quad (19)$$

Solutions do not exist under quite a wide range of conditions. This is a potentially fatal impediment.

It may be possible to reformulate the locally linear problem to avoid these difficulties. Those time steps where there is no solution might be accommodated by the solution of Eq. (14) in the least-squares sense rather than an exact solution. It may also be advisable to use neighboring observations in the local solutions. From the experience of the Sobey (1992) locally nonlinear solution from water surface traces, both of these measures might help in dealing with observational error bands. All of these, however, increase the complexity of the locally linear formulation and negate the sole advantage of a linear formulation, simplicity. A locally nonlinear analysis is viable and is introduced in Section 4.

4. A local nonlinear analysis

Nonlinear and irregular waves follow a field equation, the Laplace equation:

$$\frac{\partial^2\phi}{\partial x_\alpha \partial x_\alpha} + \frac{\partial^2\phi}{\partial z^2} = 0, \quad (20)$$

together with kinematic and dynamic free surface boundary conditions:

$$f'_{\text{K}} = w - \frac{\partial\eta}{\partial t} - u_\alpha\frac{\partial\eta}{\partial x_\alpha} = 0 \text{ at } z = \eta, \quad (21)$$

$$f_{\text{D}} = \frac{\partial\phi}{\partial t} + \frac{1}{2}\left(u_\beta u_\beta + w^2\right) + g\eta = 0 \text{ at } z = \eta, \quad (22)$$

and a kinematic bottom boundary condition on a sloping bed:

$$w + u_\alpha\frac{\partial h}{\partial x_\alpha} = 0 \text{ at } z = -h. \quad (23)$$

These equations assume only that the flow is irrotational and incompressible. The velocity potential function is defined such that the velocity components are $(u_\alpha, w) = (\partial\phi/\partial x_\alpha, \partial\phi/\partial z)$.

If it is further assumed that the bottom is locally horizontal, the bottom boundary condition becomes just:

$$w = 0 \text{ at } z = -h. \tag{24}$$

Nonlinear wave solutions of the form:

$$\phi(x_\alpha, z, t) = U_\alpha x_\alpha + \sum_j A_j \frac{\cosh jk(h+z)}{\cosh jkh} \sin j(k_\alpha x_\alpha - \omega t), \tag{25}$$

exactly satisfy the field (Eq. (20)) and the reduced bottom boundary condition (Eq. (24)). The current U_α must be steady and depth-uniform, excluding any consideration of velocity shear.

From the known velocity potential function, the velocity components are:

$$u_\alpha(x_\alpha, z, t) = U_\alpha + \sum_j jk_\alpha A_j \frac{\cosh jk(h+z)}{\cosh jkh} \cos j(k_\alpha x_\alpha - \omega t), \tag{26}$$

$$w(x_\alpha, z, t) = \sum_j jkA_j \frac{\sinh jk(h+z)}{\cosh jkh} \sin j(k_\alpha x_\alpha - \omega t). \tag{27}$$

Using also the irrotational Bernoulli equation, the dynamic pressure is:

$$p_\mathrm{d}(x_\alpha, z, t) = \bar{B} - \frac{\partial\phi}{\partial t} - \frac{1}{2}\left(u_\alpha u_\alpha + w^2\right), \tag{28}$$

in which:

$$\frac{\partial\phi}{\partial t} = -\sum_j j\omega A_j \frac{\sinh jk(h+z)}{\cosh jkh} \cos j(k_\alpha x_\alpha - \omega t), \tag{29}$$

and the Bernoulli constant is (Sobey, 1992):

$$\bar{B} = \frac{1}{2} U_\alpha U_\alpha + \frac{1}{4} \sum_j \left(\frac{jkA_j}{\cosh jkh} \right)^2. \tag{30}$$

A prediction of the local kinematics is sought throughout the water column in the immediate neighborhood of the PUV gauge at horizontal position x_α. The pressure sensor is at known elevation z_P and the directional current meter at known elevation z_UV. Measured dynamic pressure traces $p_\mathrm{d}^\mathrm{obs} = p_\mathrm{d}(t_i; x_\alpha, z_\mathrm{P})$ are available at discrete times t_i, and measured velocity component traces $u_\alpha^\mathrm{obs} = u_\alpha(t_i; x_\alpha, z_\mathrm{UV})$ are available at the same discrete times. The local water depth h and depth-uniform current U_α are also known. The current can be estimated from the UV traces as a time-average over sufficient time to average over the local waves but not over local astronomical and storm tide currents.

The unknowns in this local solution are radian frequency ω, the wave number components k_α, the spatial phase $k_\alpha x_\alpha$, the Fourier coefficients A_j and the local water

surface elevations $\eta_n = \eta(t_n; x_\alpha)$ in the neighborhood of time t_i. With J Fourier coefficients, N local water surface elevations, and treating the spatial phase as a single unknown, there are $4 + J + N$ unknowns.

Active equations are provided by the PUV observations and by the kinematic and dynamic free surface boundary conditions. Note that the primitive form of the kinematic free surface boundary condition, Eq. (21), requires estimates of $\partial\eta/\partial t$ and $\partial\eta/\partial x_\alpha$. The temporal gradient $\partial\eta/\partial t$ might be estimated from interpolation among the local η_n which is part of the solution, but there is no spatial information from the PUV traces. Sobey (1992) estimated these spatial gradients by imposing a locally steady approximation on the waves.

This additional approximation can be avoided. The problem formulation is not compromised by redefinition (Longuet-Higgins, 1962) of the kinematic free surface boundary condition as:

$$\begin{aligned} f_{\mathrm{K}} &= f'_{\mathrm{K}} + \frac{1}{g}\frac{Df_{\mathrm{D}}}{Dt} \\ &= w + \frac{1}{g}\frac{D}{Dt}\left(\frac{\partial\phi}{\partial t}\right) + \frac{u_\beta}{g}\frac{Du_\beta}{Dt} + \frac{w}{g}\frac{Dw}{Dt} \text{ at } z = \eta. \end{aligned} \tag{31}$$

This modified form of the kinematic free surface boundary condition excludes both temporal and spatial gradients of η.

As an initial evaluation of this form of the kinematic free surface boundary condition, it was substituted in the Sobey (1992) code for local irregular wave kinematics from a single water surface trace (local Fourier irregular; LFI-E). For theoretical traces where the locally steady approximation was exact, the results were visually identical. For measured traces, the results were similar. Without the need to estimate $\partial\eta/\partial t$ from measured water surface elevations, the local numerical solutions appeared to be much more robust. The Eq. (31) form of the kinematic free surface boundary condition was adopted in the present PUV analysis.

At any time t where there is an assigned water surface node, active theoretical equations are provided by both free surface boundary conditions. In addition, there are PUV observational equations at each discrete measurement time t_i. Each of these equations are implicit and algebraic. Available equations are the modified KFSBC at η, the DFSBC at η, a pressure equation at z_{P} and two horizontal velocity equations at z_{UV}:

$$\begin{aligned} &f_{\mathrm{K}}(\omega, k_\alpha, k_\alpha x_\alpha, A_j, \eta) = w + \frac{1}{g}\frac{D}{Dt}\left(\frac{\partial\phi}{\partial t}\right) + \frac{u_\beta}{g}\frac{Du_\beta}{Dt} + \frac{w}{g}\frac{Dw}{Dt} = 0 \text{ at } z = \eta \\ &f_{\mathrm{D}}(\omega, k_\alpha, k_\alpha x_\alpha, A_j, \eta) = \frac{\partial\phi}{\partial t} + \frac{1}{2}\left(u_\beta^2 + w^2\right) + g\eta = 0 \text{ at } z = \eta \\ &f_p(\omega, k_\alpha, k_\alpha x_\alpha, A_j, \eta) = p_{\mathrm{d}} - p_{\mathrm{d}}^{\mathrm{obs}} = 0 \text{ at } z = z_{\mathrm{P}} \\ &f_{u_\alpha}(\omega, k_\alpha, k_\alpha x_\alpha, A_j, \eta) = u_\alpha - u_\alpha^{\mathrm{obs}} = 0 \text{ at } z = z_{\mathrm{UV}}. \end{aligned} \tag{32}$$

Additional closure equations can be provided by observational and free surface boundary equations at neighboring times within a short local window of duration τ_0 that is centered on t_i. At least $4+J+N$ independent equations must be provided to solve for $4+J+N$ unknowns.

Apart from this strict mathematical closure requirement, there is an additional constraint. The K and D free surface boundary equations are exact, but the P, U and V observational equations have measurement error bands. Also, the P and U, V sensors are unlikely to have the same accuracy. Present technology has much larger error bands on the U, V traces than on the P traces; this is seen quite clearly in Fig. 2b, where the sampling rate is 4 Hz. These realities of the problem formulation are accommodated by a significant overspecification of the problem, especially with the UV observational equations, and the adoption of a least squares rather than an exact solution. Flexibility in the time location of the PUV observational equations was also introduced through cubic spline interpolation among the measured points.

The local LFI-PUV theory has three free parameters, the truncation order J and the number of η points N in each local window together with the width τ_0/T_z of the local windows. The truncation order has much the same authority as order in an analytical wave theory (Stokes, conoidal) or truncation order in Fourier wave theory. A window width of $\tau_0/T_z=1$ would be a global solution. A particular solution will be designated LFI-PUV[$J,N,\tau_0/T_z$]. For example, LFI-PUV[3,3,0.1] has $J=3$, $N=3$ and $\tau_0/T_z=0.1$.

5. Numerical implementation

As in Sobey (1992), the analysis segment routinely adopted was a double wave sequence centered about a crest suggested by the pressure trace. Solutions are sought in narrow local windows, with a target width of order $\tau_0=0.1T_z$, where T_z is the zero-up crossing period of the record segment.

In all applications of the present theory, it has proven convenient to assign an odd number of local water surface elevation $\eta(t_n)$; with $N=1$ or 3 (for a single width window) or 5 (for a double width window), such that there is always a computed water surface elevation centrally located in the window. With respect to the time at the center of a window of width τ_0, $\eta(t_n)$ points are located at $t/\tau_0=0$; ± 0.5; ± 1.0. K and D equations are applied at each of these $\eta(t_n)$ points, depending on the value of N. At $N=5$, the local window width is doubled. There are $2N=2$ or 6 (for a single-width window) or 10 (for a double-width window) of these water surface equations.

P, U and V observational equations are located at the center of the window. Additional PUV equations within the window are located such that UV observational equations are not assigned a weighting that was inconsistent with their routinely larger error bands. With respect to the time at the center of a window of width τ_0, P equations are located at $t/\tau_0=\pm 0.25$, ± 0.5 in a single width window and also at ± 0.75, ± 1 in a double width window. The associated U and V equations are located at $t/\tau_0=\pm 0.125$, ± 0.25, ± 0.375, ± 0.5 in a single-width window and also ± 0.625, ± 0.75, ± 0.875, ± 1 in a double-width window. The explicit higher density of UV equations, together

with the least squares algorithm, was adopted as partial accommodation of the larger error bands of the UV observational equations. The least squares objective function was normalized as:

$$O(\omega, k_\alpha, k_\alpha x_\alpha; A_j; \eta_n) = \frac{1}{2N}\Sigma\left(f_{\mathrm{K}}^2 + f_{\mathrm{D}}^2\right) + \frac{1}{N_{\mathrm{P}}}\Sigma f_{\mathrm{P}}^2 + \frac{1}{2N_{\mathrm{UV}}}\Sigma\left(f_{\mathrm{U}}^2 + f_{\mathrm{V}}^2\right), \tag{33}$$

such that K, D, P and UV equation groups have equal weight. N_{P} is $1 + 4L$ and N_{UV} is $1 + 8L$, where L is 1 (single-width window) or 2 (double-width window).

There are $3 + 20L = 23$ (for a single width window) or 43 (for a double width window) observational equations. There are a total of $2N + 3 + 20L$ physical and observational equations in $4 + J + N$ unknowns, where $2N + 3 + 20L$ must equal or exceed $4 + J + N$. A typical application has $J = 3$ and $N = 3$, so that there are 10 unknowns: $\omega, k_\alpha, k_\alpha x_\alpha, A_1, A_2, A_3, \eta_1, \eta_2, \eta_3$. For a single-width window, there are 29 equations, and 49 for a double-width window. Experience suggested that this level of overspecification was generally necessary to accommodate the observational error bands. For theoretical wave traces with no observational error bands (see Section 6), only a closed set of KD and PUV equations was necessary for credible solutions; overspecification did not compromise this success.

The problem formulation requires the least-squares solution of a system of simultaneous, nonlinear, implicit algebraic equations. Numerical solutions routinely used the Dennis et al. (1981b) NL2SOL code; an updated code is available from the internet Netlib repository of scientific subroutines in fortran. The algorithm (Dennis et al., 1981a) is a variation on Newton's method in which part of the Hessian matrix is computed exactly and part is approximated by a secant updating method. To promote convergence from poor starting guesses, a model/trust-region technique is used along with an adaptive choice of the model Hessian. In operation, the algorithm sometimes reduces to the classical Gauss–Newton or Levenberg–Marquardt methods.

The number of unknowns, typically 10, is relatively large. In any such high order nonlinear optimization problem, the crucial elements of successful solutions are invariably accurate estimates of the Jacobian and good initial solution estimates. Accurate estimates of the Jacobian require analytical estimates of the partial derivatives of all f equations with respect to all the unknown parameters. These are the quantities $\partial f_{\mathrm{K}}/\partial\omega, \partial f_{\mathrm{K}}/\partial k_1, \partial f_{\mathrm{K}}/\partial k_2, \ldots$ through $\ldots, \partial f_{u_2}/\partial\eta_N$. The analytical derivatives were evaluated and confirmed against finite difference approximations.

Establishing good initial solution estimates always requires extensive experience with the particular physical problem and system of equations. The methodology finally adopted was a two-stage algorithm. The initial step identified three overlapping record sub-segments, the half-wave extract centered on the leading trough, the half-wave centered on the central crest and the half-wave centered on the following trough. Each half-wave is equivalent to an extra-wide window of width about $0.5T_z$. In each half-wave of, say, $\mathscr{N}$ discrete PUV observations, η points were located at the same times such that there are $4 + J + \mathscr{N}$ unknowns. K, D, P, U and V equations are assigned at the same times, giving $5\mathscr{N}$ equations. For a PUV record sampled at $\mathscr{s}$ Hz, there

would be about $7\mathscr{J}$ observational points in a half-window. For $J = 3$ and $\mathscr{J} = 1$, there would be 14 unknowns and 35 equations. For $J = 3$ and $\mathscr{J} = 4$, there would be 35 unknowns and 140 equations. With initial estimates provided by a global Airy theory approximation, smooth and robust solutions are established in each extra-wide half-window. These in turn provide routinely appropriate initial estimates for the local solutions in very much narrower windows.

The algorithm had most difficulty in finding credible local solutions around the zero-crossings of the P trace. At such regions, profile curvature is very small and a narrow local window has poor resolution. Often, this is not a region of particular concern. Two strategies are possible in dealing with this problem. The first would be to ignore such points and rely on interpolating for the kinematics from adjacent local solutions that bracket the zero-crossings. The second would be to extend the local window to improve resolution of the local profile curvature. This second approach has been adopted, and was the essential rationale for the double-width window introduced above.

6. Theoretical wave traces

An initial evaluation of the LFI-PUV theory and coding is provided by theoretical PUV traces from uniform, long-crested wave trains. Three monochromatic waves,

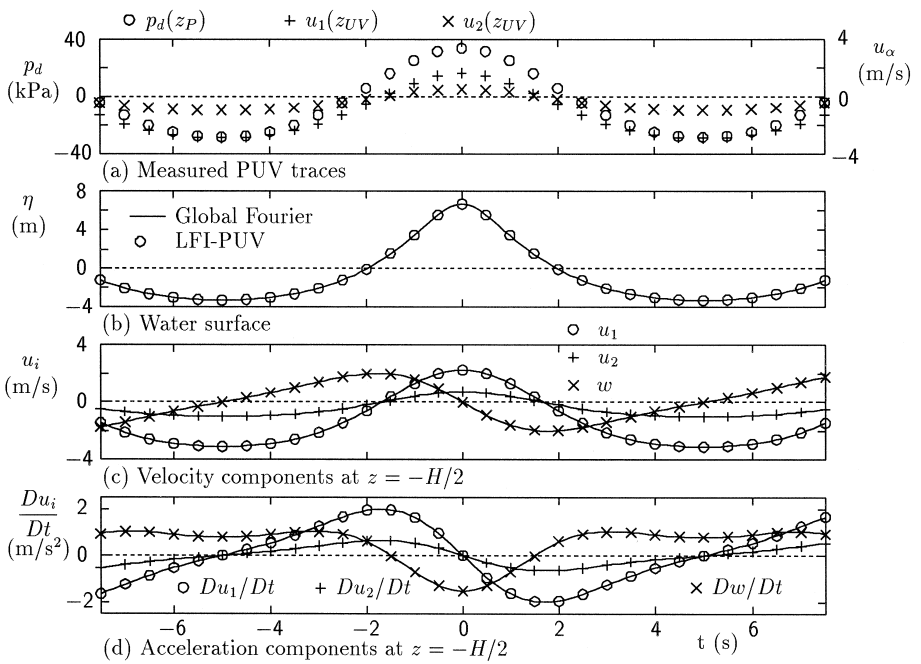

Fig. 4. LFI-PUV[3,3,0.1] predictions for wave 'Twenty'.

'Five', 'Twenty' and 'Hundred', have been defined, respectively, in wave shallow, wave transitional and wave deep water. The details are listed in Table 1. The wave heights in all three cases are moderately extreme for the depth. Note in particular the location of both z_P and z_{UV} higher in the water column for waves 'Twenty' and 'Hundred'. The significant attenuation in wave kinematics with depth is frequently mitigated by such a practice. Global Fourier wave theory (Sobey, 1989), at truncation order 18 with 25 water surface nodes from crest to trough, provides near-exact kinematics for these wave trains.

The PUV observational traces at the listed elevations were predicted at a time interval of 0.5 s. LFI-PUV[3,3,0.1] predictions for wave 'Twenty' are shown in Fig. 4. Part (a) shows the 'measured' $p_d(t;z_P)$ trace together with the 'measured' $u_1(t;z_{UV})$ and $u_2(t;z_{UV})$ traces. Part (b) shows the η traces predicted by LFI-PUV (markers) and by the near-exact Fourier wave theory (continuous line). Compare this result to the relatively poor prediction of η for wave 'Twenty' using the locally linear method (Fig. 3). Part (c) shows all three velocity components at elevation $z = -H/2$ just below the trough, and part (d) all three acceleration components also at the same near trough elevation. Again, the markers are LFI-PUV predictions and the continuous lines are from the near-exact Fourier wave theory. Agreement throughout is almost perfect.

The excellent agreement is achieved at a relatively low order ($J = 3$), and this is a consistent strength of the LFI methodology. This success at such low order is achieved by seeking separate solutions in each local window. The solution parameters, $\omega, k_\alpha, k_\alpha x_\alpha, A_j, \eta_n$, will vary from window to window. The variation in the ω, k_α and A_j parameters, that would also be defined in a global solution, is not expected to be very large. The local variation in these solution parameters for wave 'Twenty' is shown in Fig. 5. Note the double-width windows at the profile zero-crossings near $t = \pm 2$ s.

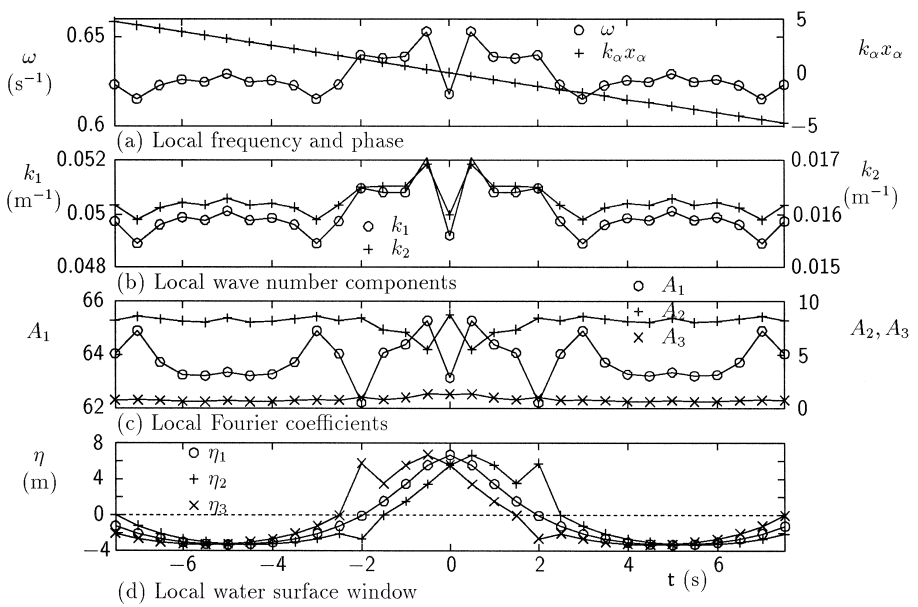

Fig. 5. LFI-PUV[3,3,0.1] local solution parameters for wave 'Twenty'.

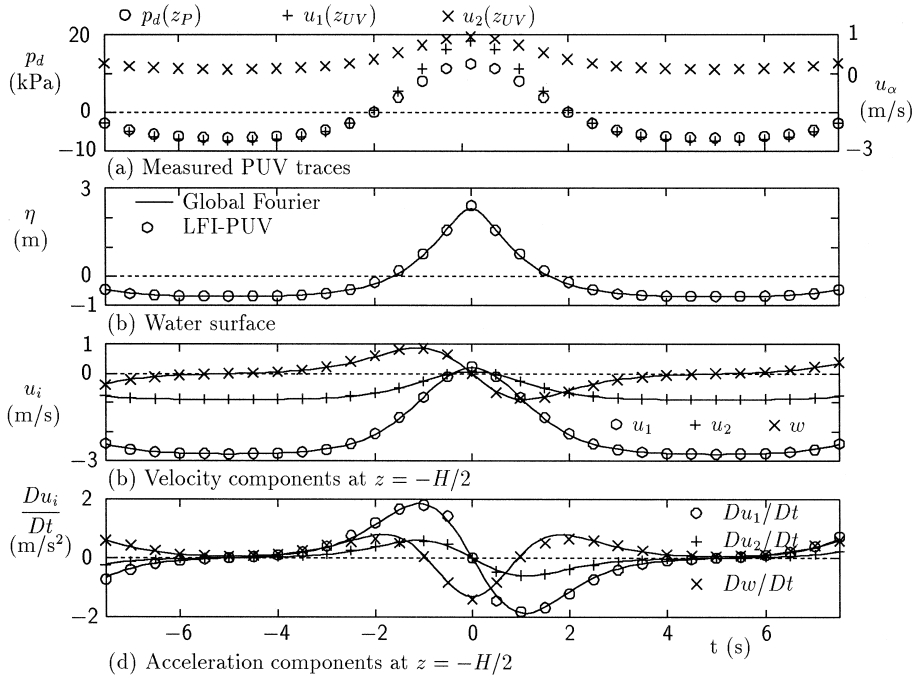

Fig. 6. LFI-PUV[3,3,0.1] predictions for wave 'Five'.

Similarly excellent agreement is achieved for waves 'Five' and 'Hundred', respectively, in wave shallow and wave deep water. Comparisons of LFI-PUV[3,3,0.1] solutions and near-exact Fourier kinematics are shown in Figs. 6 and 7. Collectively, waves 'Five', 'Twenty' and 'Hundred' demonstrate the suitability of the LFI-PUV algorithm under expected operational conditions from wave shallow through wave transitional to wave deep water.

7. Measured wave traces

The theoretical traces of Section 6 provide confidence in the problem formulation and in the numerical algorithm. But the LFI-PUV methodology is intended for the nonlinear interpretation of field PUV traces. The inherent measurement error bands of field PUV traces will provide a much more challenging test.

The two field records partially illustrated in Fig. 2 have been used for evaluation. Apart from sampling very different wave climates, these records differ very significantly in the sampling rates, 1 Hz for the Platform Edith data and 4 Hz for the Columbia River data.

Figs. 8 and 9 show sample LFI-PUV[3,3,0.2] predictions of local kinematics from these records. These predictions are credible and they match the measured PUV traces by definition, but there is no independent field data for confirmation. In the Sobey

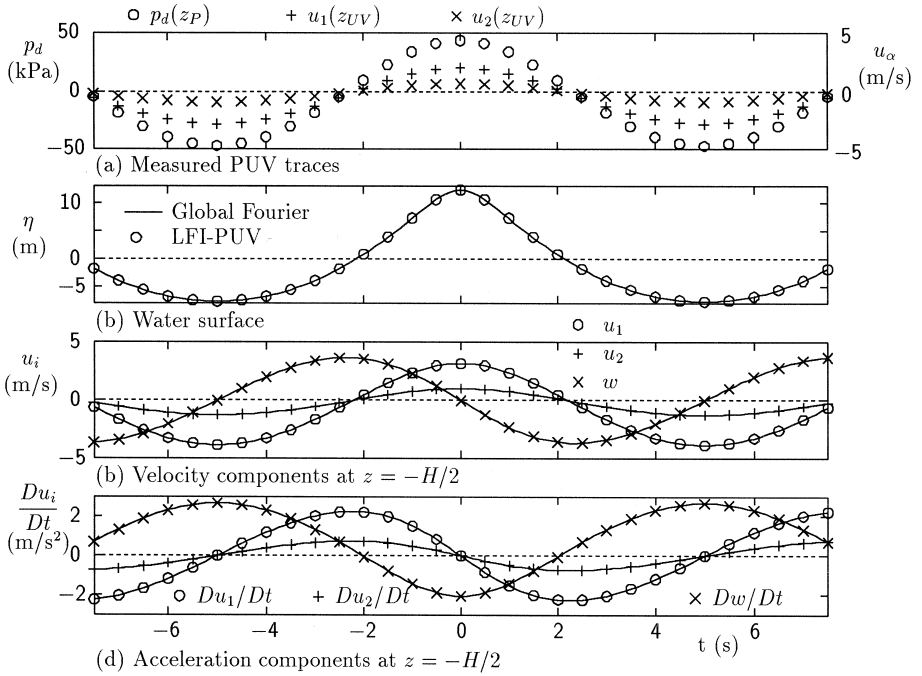

Fig. 7. LFI-PUV[3,3,0.1] predictions for wave 'Hundred'.

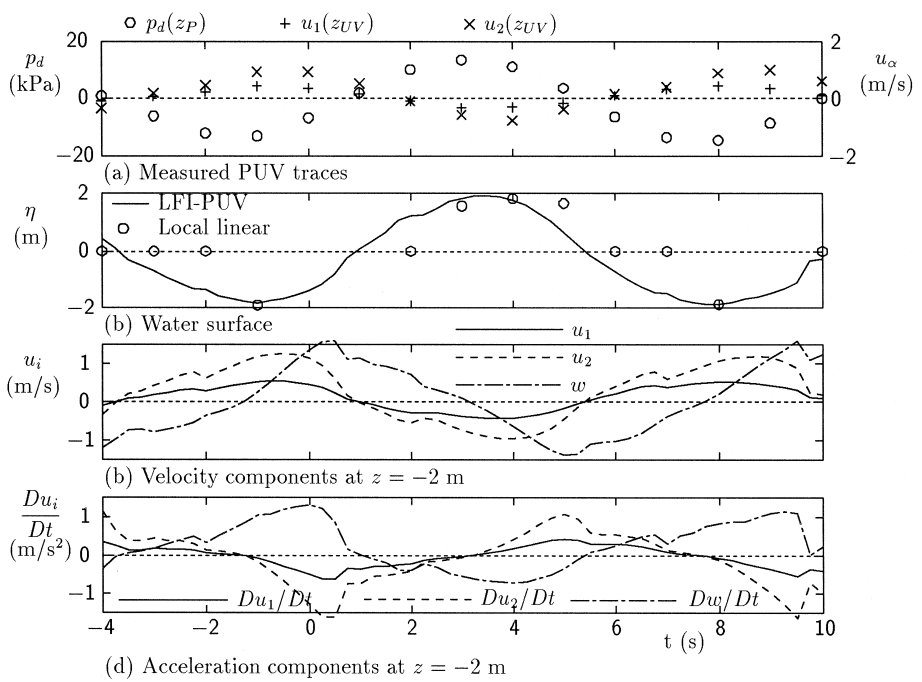

Fig. 8. LFI-PUV[3,3,0.2] predictions from Platform Edith data.

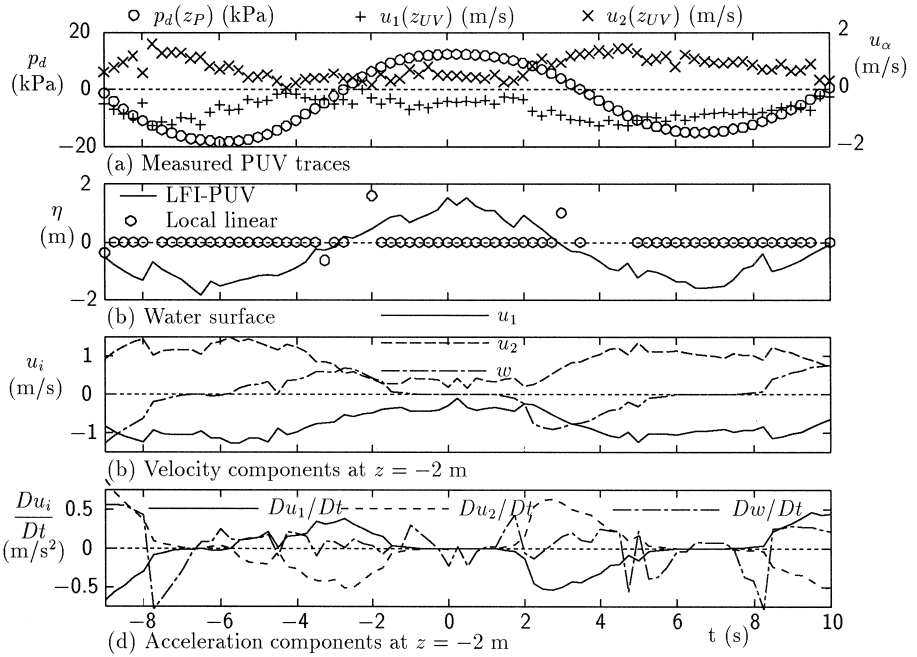

Fig. 9. LFI-PUV[3,3,0.2] predictions from Columbia River data.

(1992) LFI-E theory for irregular wave kinematics from single-point water surface traces, a window width of $\tau_0/T_z = 0.1$ was routinely satisfactory. For PUV traces, the observational equations are somewhat less authoritative. An obvious reason is the relatively large error bands on the UV measurements. Another possible reason is natural signal attenuation with depth of submergence; the higher frequencies are most rapidly attenuated and their influence may get lost in the error bands (Barker, 1998). Nevertheless, experience suggested the routine adoption of a slightly wider window width of $\tau_0/T_z = 0.2$. Barker and Sobey (1996) also recommended this same window width for irregular wave kinematics from pressure records alone.

It is instructive, nevertheless, to compare the locally nonlinear prediction of sea surface elevation with the locally linear prediction (shown as the markers on Figs. 8b and 9b). The density of the linear solutions match the data resolution. In Fig. 8b, Δt is 1.0 s. Where there is no solution (see Eq. (17) and following), the marker is located at the MWL, as at times -4, -3 -2, 2, 6, 7 and 10 s. Solutions at 0, 1 and 9 s are significantly off scale, and only those at -1, 3, 4, 5 and 8 s have any credibility. In Fig. 9b, Δt is 0.25 s. There are many 'no solution' markers and the few locations where linear solutions were obtained are mostly off-scale or have little credibility. The theoretical reservation on the linear method, potentially significant underprediction at the crest (see Fig. 3), is clearly overwhelmed by the frequency of either 'no solution' results or solutions that have no visual credibility. The linear method must be rejected on both theoretical and practical grounds.

The LFI-PUV solutions for the Columbia River data have a somewhat tenuous nature, evidenced by the sharp changes in predicted kinematics in the neighborhood of times -8, $+5$ and $+8$ s. The UV error bands for this record (Fig. 2b) are quite significant. The specific PUV gauge was designed with the expectation that analysis would follow the Longuet-Higgins et al. (1963) linear and global frequency-domain analysis outlined in Eqs. (1)–(10). In this global linear analysis, measurement error is easily accommodated by spectral smoothing of the $E_{pu_1}(\omega,\theta)$ through $E_{u_2u_2}(\omega,\theta)$ auto-variance and cross-variance spectra and/or the $E_{\eta\eta}(\omega,\theta)$ estimate from Eq. (7).

Measurement error bands are not so easily dismissed in the local LFI-PUV theory. LFI-PUV seeks an enhanced representation of the local kinematics, through the direct use of local PUV measurements in the problem formulation. The local PUV measurements provide the local reality, so that the predictive potential can be significantly compromised by local measurement error. The Columbia River data set provides a useful reality check. While the value of the Fig. 9 predictions are arguably tenuous, their particular value may lie in the identification of UV measurement error bands as a relevant design issue for PUV instrumentation.

An associated instrument design issue is the attenuation of the fluctuating kinematics (P and UV) with increasing depth of submergence and with increasing frequency. The attenuation increases with both frequency and depth of submergence. Transducer accuracy is absolute, so that relative accuracy is significantly compromised for deeply submerged instruments at higher frequencies in deeper water. There is only partial mitigation for this in the superior accuracy of P measurements, with respect to UV measurements. The design compromise has been to locate PUV gauges reasonably high in the water column to avoid this problem as much as possible. The Columbia River gauge is deployed at -16.8 m where the water depth is 17.6 m, but the Platform Edith gauge is deployed at only -7.4 m where the water depth is 46 m. The deeper submergence of the Columbia River gauge contributes to the tenuous nature of the analysis of this data.

A careful review of the Fig. 9 predictions reveals that the maximum vertical velocity prediction, 1.59 m/s at $+0.5$ s, exceeds the maximum horizontal velocity prediction, 1.39 m/s at -0.5 s. In a global steady wave solution, such as the 'global Fourier' solutions in Figs. 4, 6 and 7, the maximum horizontal and vertical velocities will again not coincide in time, but the maximum vertical velocity magnitude will always be smaller than the maximum horizontal velocity magnitude. This underlines the local character of the LFI-PUV methodology. The LFI-PUV solutions in each local window are independent, and directly reflect the local measured kinematics. There is no global influence.

A final phase in evaluation of the LFI-PUV methodology would be detailed laboratory measurements of kinematics under regular and irregular wave conditions. These should include a PUV instrument plus the local water surface and (u_α,w) velocity component and dynamic pressure measurements at one or more different near-surface elevations. Suitable laboratory data do not presently exist. Establishing a suitable data set would be a very major task. It would presumably involve sophisticated three-dimensional laser Doppler instrumentation for the velocity measurements. Pressure is very rarely measured in a wave laboratory, except at structures where the data would be

unsuitable. Pressure measurement at near-surface elevations under waves would require special attention.

8. Conclusions

Traditional directional analysis of PUV data results in linearized estimates of directional wave and velocity spectra which typically do not include steady currents. Attempts to reconstitute velocity time series at any other location in the water column result in linear estimates with decreasing veracity approaching the free surface. The single advantage of linear directional spectral analysis is the compactness of the output which corresponds to loss of information. However, this compactness could become a liability in some applications.

A new method has been presented for interpreting traces recorded by conventional PUV instruments under irregular multidirectional waves. This time-domain method provides estimates of sea surface elevation and wave kinematics throughout the water column without compromising the essential nonlinear character of the waves. The key to the formulation is retention of the fully nonlinear free surface boundary conditions which are used in seeking a nonlinear least-squares solution in a narrow time window. Also included is the nonlinear interaction between the waves and a steady and depth-uniform current. The analysis method provides nearly exact results for theoretical nonlinear steady waves. Application to field data requires overspecification in the solution to allow for instrument error bands. Nevertheless, credible solutions were obtained using PUV measurement from two field locations with very energetic wave and current conditions.

Results from the locally nonlinear analysis differ substantially from traditional directional spectra. The method provides time series of sea surface elevation η, radial frequency ω, directional wave numbers k_1 and k_2, and Fourier coefficients, A_j. These local solution parameters provide predictions of corresponding time series for any kinematic quantity at any position in the water column. A complete field solution is available at each time interval.

The locally nonlinear PUV method provides a distinct improvement for analyzing practical problems in which individual wave characteristics are critical. For example, wave loads on offshore structures depend on wave height, fluid velocity, fluid acceleration, and the phasing between maximum velocity and acceleration. Retaining the nonlinear characteristics inherent in the measured data is critical for credible load determination.

The locally nonlinear analysis is fairly computationally intensive, and it creates additional information rather than condensing the measurements. Therefore, this method is probably not well-suited for routine analysis and archiving of PUV records obtained over a lengthy deployment. However, because the method does not rely on the entire time series, it is possible to perform selective analysis of individual waves or large wave groups within the time series that may be of particular interest. Examples include so-called ‘freak waves’ and even tsunami waves. Also, the local nature of the nonlinear analysis method may find application providing near real-time wave estimates from

PUV gauges. It may also assist in the design evolution of PUV gauges, as it provides a more realistic interpretation of the strong nonlinearities associated with the more extreme events.

Acknowledgements

The research described and the results presented herein, unless otherwise noted, were obtained from research funded through the *Scour Holes at Inlet Structures* work unit in the *Coastal Inlets Research Program* at the US Army Engineer Waterways Experiment Station (WES). Mr. Patrick McKinney of WES provided the Platform Edith PUV data. The Columbia River PUV data were collected as part of the *Mouth of Columbia River* work unit of the *Monitoring of Completed Navigation Projects Program* of the US Army Corps of Engineers. Permission to publish this information was granted by the Chief of Engineers.

References

Barker, C.H., 1998. Directional irregular wave kinematics. PhD thesis, University of California at Berkeley, available from University Microfilms.

Barker, C.H., Sobey, R.J., 1996. Irregular wave kinematics from a pressure record. In: Edge, B.L. (Ed.), 25th Coastal Engineering Conference, Orlando, Vol. 1. ASCE, New York, pp. 1034–1047.

Dennis, J.E., Gay, D.M., Welsch, R.E., 1981a. An adaptive nonlinear least-squares algorithm. ACM Transactions on Mathematical Software, pp. 348–368.

Dennis, J.E., Gay, D.M., Welsch, R.E., 1981b. Algorithm 573 NL2SOL—an adaptive nonlinear least-squares algorithm. ACM Transactions on Mathematical Software, pp. 369–383.

Grosskopf, W.G., Aubrey, D.G., Mattie, M.G., Mathiesen, M., 1983. Field intercomparison of nearshore directional wave sensors. IEEE Journal of Oceanic Engineering 255–271.

Horikawa, K., 1988. Nearshore Dynamics and Coastal Processes. University of Tokyo Press, Tokyo.

Lee, D.-Y., Wang, H., 1984. Measurement of surface waves from subsurface gage. In: Edge, B.L. (Ed.), Proc. 19th Coastal Engineering Conference, Houston, Vol. 1. ASCE, New York, pp. 271–286.

Longuet-Higgins, M.S., 1962. Resonant interactions between two trains of gravity waves. Journal of Fluid Mechanics 12, 321–332.

Longuet-Higgins, M.S., Cartwright, D.E., Smith N.D., 1963. Observations of the directional spectrum of sea waves using the motions of a floating buoy. In: Ocean Wave Spectra, Proceedings of a Conference at Easton MD, May 1961. Prentice-Hall, Englewood Cliffs, NJ, pp. 111–136.

Nielsen, P., 1989. Analysis of natural waves by local approximations. Journal of Waterway, Port, Coastal and Ocean Engineering 115, 384–396.

Sobey, R.J., 1989. Variations on Fourier wave theory. International Journal for Numerical Methods in Fluids 9, 1453–1467.

Sobey, R.J., 1992. A local Fourier approximation method for irregular wave kinematics. Applied Ocean Research 14, 93–105.